

Reinterpreting Shock Wave Structure Predictions using the Navier-Stokes Equations

M. H. Lakshminarayana Reddy* and S. Kokou Dadzie†

School of Engineering and Physical Sciences, Heriot-Watt University, Edinburgh EH14 4AS, Scotland, UK

Classical Navier-Stokes equations fail to predict shock wave profiles accurately. In this paper, the Navier-Stokes system is fully transformed using a velocity variable transformation. The transformed equations termed the re-casted Navier-Stokes equations display physics not initially included. We then analyse the stationary shock structure problem in a monatomic gas by solving both the classical and the re-casted Navier-Stokes equations numerically using a finite difference global solution (FDGS) scheme. The numerical results are presented for different upstream Mach numbers ranging from supersonic to hypersonic flows. We found that the re-casted Navier-Stokes equations show better agreements with the experimentally measured density and reciprocal shock thickness profiles.

I. INTRODUCTION

One of the best-known example of a simple and highly non-equilibrium compressible flow phenomena is that of a normal shock wave. A normal shock wave is a disturbance propagating between a supersonic fluid and a subsonic fluid, characterized by a sharp change in its fluid properties. In other words, one can treat the shock wave as an interface of finite thickness between two different equilibrium states of a gas [1–5]. Shock waves arise at explosions, detonations, supersonic movements of bodies, and so on. The shock structure problem has been studied extensively in the middle of the 20th century using theoretical, numerical and experimental techniques. It now serves as a standard benchmark problem for testing the capability (validity) and accuracy of different hydrodynamics and extended hydrodynamic fluid flow models [6, 7]. A few advantages of a shock structure problem making it attractive for numerical simulations are: (i) its one-dimensional and steady state; (ii) the upstream and downstream boundary conditions are clearly specified by the Rankine-Hugoniot conditions; (iii) all gradients of hydrodynamic field variables vanish far upstream and downstream of the shock; and (iv) solid boundaries are absent [8].

The principal parameter used to classify the non-equilibrium state of a rarefied flow is the Knudsen number, Kn . It is defined as the ratio of the mean free path of the gas molecules to the characteristic length of the flow system. In the shock structure problem, Kn is related to the shock thickness [6]. Within a shock layer, physical properties of the gas change very fast over a distance of a few mean free paths which makes the Knudsen number large. Typical values of the Knudsen number for a flow within a shock layer fall between ≈ 0.2 and ≈ 0.3 [6]. These are beyond the classical continuum- Kn regime and fall into the so-called ‘intermediate- Kn ’ regime ($0.01 \lesssim Kn \lesssim 1$). Hence shock structures are not well captured by standard fluid dynamic equations. In particular, shock structure predictions from standard Navier-Stokes equations have shown some agreements with the experimental data at very low Mach numbers $Ma_1 < 1.5$ but clearly failed about Mach number of 2 [9]. Deriving appropriate continuum models that can predict these data is still therefore an active research topic [10].

In this article, a method is used to reinterpret the original Navier-Stokes equations and its prediction of the experimental data. A change of velocity variable is used to transform the equations into physically different equations before they are solved to compare with the experimental data.

The paper is folded as follows: in §II we briefly present the classical hydrodynamic equations of fluid flows along with the new strategy to obtain a new continuum hydrodynamic model, namely, the re-casted Navier-Stokes equations. In the following section §III, both hydrodynamic models are reduced to one-dimensional stationary shock structure problem and then solved numerically using a finite difference global solution scheme (FDGS). Predictions of shock structures by both models are presented and compared with existing experimental and DSMC data in §IV. At the end conclusions are presented.

II. THE CLASSICAL AND THE RE-CASTED NAVIER-STOKES EQUATIONS

Our new theory starts with the classical Navier-Stokes-Fourier equations which are a differential form of the three classical conservation laws, namely, mass, momentum and energy conservation laws that govern the motion of a fluid. In an Eulerian reference frame they are:

* l.mh@hw.ac.uk

† k.dadzie@hw.ac.uk

mass balance equation

$$\frac{\partial \rho}{\partial t} + \nabla \cdot [\rho U] = 0, \quad (1)$$

momentum balance equation

$$\frac{\partial \rho U}{\partial t} + \nabla \cdot [\rho U \otimes U] + \nabla \cdot [p \mathbf{I} + \mathbf{\Pi}^{(NS)}] = 0, \quad (2)$$

energy balance equation

$$\frac{\partial}{\partial t} \left[\frac{1}{2} \rho U^2 + \rho \mathbf{e}_{in} \right] + \nabla \cdot \left[\frac{1}{2} \rho U^2 U + \rho \mathbf{e}_{in} U \right] + \nabla \cdot [(p \mathbf{I} + \mathbf{\Pi}^{(NS)}) \cdot U] + \nabla \cdot \mathbf{q}^{(NS)} = 0, \quad (3)$$

where ρ is the mass-density of the fluid, U is the flow mass velocity, p is the hydrostatic pressure, \mathbf{e}_{in} is the specific internal energy of the fluid, $\mathbf{\Pi}^{(NS)}$ is the shear stress tensor, \mathbf{I} is the identity tensor and $\mathbf{q}^{(NS)}$ is the heat flux vector. All these hydrodynamic fields are functions of time t and spatial variable \mathbf{X} . Additionally, ∇ and $\nabla \cdot$ denote the usual spatial gradient and divergence operators, respectively, while the operator \otimes denotes usual tensor product of two vectors. Expression for the specific internal energy is given by, $\mathbf{e}_{in} = p/\rho(\gamma - 1)$ with γ being the isentropic exponent. The constitutive models for the shear stress $\mathbf{\Pi}^{(NS)}$ and the heat flux vector $\mathbf{q}^{(NS)}$ are due to the Newton's law and the Fourier's law, respectively, and they are given by,

$$\mathbf{\Pi}^{(NS)} = -2\mu \left[\frac{1}{2} (\nabla U + \widetilde{\nabla U}) - \frac{1}{3} \mathbf{I} (\nabla \cdot U) \right] = -2\mu \overset{\circ}{\nabla U}, \quad \mathbf{q}^{(NS)} = -\kappa \nabla T, \quad (4)$$

where $\widetilde{\nabla U}$ represents the transpose of ∇U . Coefficients μ and κ are the dynamic viscosity and the heat conductivity, respectively.

The system (1) - (4) is the well-known conventional fluid flow model and is widely used to model a viscous and heat conducting fluid. Instead of solving directly this system, we first perform a transformation based on the following change of variable:

$$U = U_v - \kappa_m \nabla \ln \rho = U_v - \frac{\kappa_m}{\rho} \nabla \rho, \quad (5)$$

where κ_m is a molecular diffusivity co-efficient. Equation (5) is a relation between the fluid mass velocity and the fluid volume velocity which originates from *volume diffusion hydrodynamic theory* [11–13]. It has also been derived using a stochastic variational method [14].

Substituting equation (5) into the system (1) - (4), it transforms into a new system which we named the re-casted Navier-Stokes system and is given by:

re-casted mass balance equation

$$\frac{\partial \rho}{\partial t} + \nabla \cdot [\rho U_v - \kappa_m \nabla \rho] = 0, \quad (6)$$

re-casted momentum balance equation

$$\frac{\partial}{\partial t} [\rho U_v - \kappa_m \nabla \rho] + \nabla \cdot [\rho U_v \otimes U_v + p \mathbf{I} + \mathbf{\Pi}_v^{(RNS)}] = 0, \quad (7)$$

re-casted energy balance equation

$$\begin{aligned} & \frac{\partial}{\partial t} \left[\frac{1}{2} \rho U_v^2 + \rho \mathbf{e}_{in} - \kappa_m (\rho U_v \cdot \nabla \ln \rho) + \frac{1}{2} \kappa_m^2 (\nabla \rho \cdot \nabla \ln \rho) \right] \\ & + \nabla \cdot \left[\frac{1}{2} \rho U_v^2 U_v + \rho \mathbf{e}_{in} U_v \right] + \nabla \cdot [(p \mathbf{I} + \mathbf{\Pi}_v) \cdot U_v - \kappa_m \mathbf{\Pi}_v \cdot \nabla \ln \rho] \\ & + \nabla \cdot [\mathbf{q}_v^{(RNS)} + \kappa_m \mathcal{N}_{v1} + \kappa_m^2 \mathcal{N}_{v2} + \kappa_m^3 \mathcal{N}_{v3}] = 0, \end{aligned} \quad (8)$$

where the constitutive relations for the new shear stress and the new heat flux vector are given by,

$$\mathbf{\Pi}_v^{(RNS)} = \mathbf{\Pi}_v + \frac{\kappa_m^2}{\rho} \nabla \rho \otimes \nabla \rho - \kappa_m U_v \otimes \nabla \rho - \kappa_m \nabla \rho \otimes U_v, \quad (9)$$

$$\mathbf{q}_v^{(RNS)} = \mathbf{q}^{(NS)} - \kappa_m \rho \mathbf{e}_{in} \nabla \ln \rho - \kappa_m p \mathbf{I} \cdot \nabla \ln \rho, \quad (10)$$

$$\text{with } \mathbf{\Pi}_v = -2\mu \overset{\circ}{\nabla U_v} + 2\mu \kappa_m \widetilde{\mathbf{D}} \ln \rho - \frac{2\mu}{3} \kappa_m \Delta \ln \rho \mathbf{I}, \quad (11)$$

and \mathcal{N}_{v_i} for $i = 1$ to 3 represent other nonlinear terms which are given by,

$$\mathcal{N}_{v_1} = -(U_v \cdot \nabla \rho) U_v - \frac{1}{2} U_v^2 \nabla \rho, \quad (12)$$

$$\mathcal{N}_{v_2} = (U_v \cdot \nabla \rho) \nabla \ln \rho + \frac{1}{2\rho} |\nabla \rho|^2 U_v, \quad (13)$$

$$\mathcal{N}_{v_3} = -\frac{1}{2\rho} |\nabla \rho|^2 \nabla \ln \rho. \quad (14)$$

The operators $\tilde{\mathbf{D}}$ and Δ appearing in (11) denote the Hessian and the Laplacian operators, respectively.

Continuum flow system (6) - (8) is a type of mass diffusion hydrodynamic model. That is, it contains: (i) a mass diffusion component in the conservation of mass equation, (ii) explicit fluid dilation terms in the momentum stress tensor, and (iii) non-Fourier heat flux terms. It can be converted back into the original system (1) - (4) by reversing the change of variable in equation (5). Next, we show that the transformed system (6) - (8) may be more appropriate to solve directly for flows involving large density variations/gradients and compare directly with experimental data.

III. THE SHOCK WAVE STRUCTURE PROBLEM IN A MONATOMIC GAS

We consider a planar stationary shock wave propagating in the positive x -direction which is established in a flow of a monatomic gas. We denote the upstream ($x \rightarrow -\infty$) and downstream ($x \rightarrow \infty$) conditions of a shock, located at $x = 0$, by a subscript 1 and 2, respectively. These upstream and downstream states of the shock are connected by jump conditions: the Rankine-Hugoniot (RH) conditions [1, 15]. For this one-dimensional stationary shock flow configuration, the re-casted Navier-Stokes equations reduced to:

$$\frac{d}{dx} \left[\rho u_v - \kappa_m \frac{d\rho}{dx} \right] = 0, \quad (15)$$

$$\frac{d}{dx} \left[\rho u_v^2 + p + \Pi_v^{(RNS)} \right] = 0, \quad (16)$$

$$\frac{d}{dx} \left[\rho u_v \left(\frac{1}{2} u_v^2 + C_p T \right) + \left(\Pi_v - \frac{3}{2} \kappa_m u_v \frac{d\rho}{dx} \right) \left(u_v - \frac{\kappa_m}{\rho} \frac{d\rho}{dx} \right) - \frac{\kappa_m^3}{2\rho^2} \left(\frac{d\rho}{dx} \right)^3 + q_v^{(RNS)} \right] = 0, \quad (17)$$

with the only non-zero longitudinal new shear stress $\Pi_v^{(RNS)}$ and the new heat flux vector $q_v^{(RNS)}$ given by,

$$\Pi_v^{(RNS)} = \Pi_v - 2 \kappa_m u_v \frac{d\rho}{dx} + \frac{\kappa_m^2}{\rho} \left(\frac{d\rho}{dx} \right)^2, \quad (18)$$

$$\Pi_v = -\frac{4}{3} \mu \frac{du_v}{dx} + \frac{4}{3} \frac{\mu \kappa_m}{\rho} \frac{d^2 \rho}{dx^2} - \frac{4}{3} \frac{\mu \kappa_m}{\rho^2} \left(\frac{d\rho}{dx} \right)^2, \quad (19)$$

$$q_v^{(RNS)} = -\kappa \frac{dT}{dx} - \frac{\gamma}{(\gamma - 1)} \kappa_m \frac{p}{\rho} \frac{d\rho}{dx}. \quad (20)$$

Integration of the system (15) - (17) and later employing the ideal gas equation of state leads to:

$$\rho u_v = m_0 + \kappa_m \frac{d\rho}{dx}, \quad (21)$$

$$\rho \mathbf{R} T + \rho u_v^2 + \Pi_v^{(RNS)} = p_0, \quad (22)$$

$$\rho u_v \left(C_p T + \frac{u_v^2}{2} \right) + \left(\Pi_v - \frac{3}{2} \kappa_m u_v \frac{d\rho}{dx} \right) \left(u_v - \frac{\kappa_m}{\rho} \frac{d\rho}{dx} \right) - \frac{\kappa_m^3}{2\rho^2} \left(\frac{d\rho}{dx} \right)^3 + q_v^{(RNS)} = m_0 h_0, \quad (23)$$

where m_0, p_0 and h_0 are constants which represents the mass flow rate, the stagnation pressure and the stagnation specific enthalpy, respectively. The specific gas constant is denoted by \mathbf{R} .

In order to solve the system (21) - (23), it is convenient to work with its dimensionless form. We use the following set of dimensionless variables based on the upstream reference states (denoted with subscript 1):

$$\bar{\rho} = \frac{c_1^2}{p_1} \rho = \frac{\gamma}{\rho_1} \rho, \quad \bar{u}_v = \frac{u_v}{c_1}, \quad \bar{T} = \frac{\mathbf{R}}{c_1^2} T, \quad \bar{p} = \frac{p}{p_1}, \quad \bar{x} = \frac{x}{\lambda_1}, \quad \bar{\mu} = \frac{\mu}{\mu_1}, \quad (24)$$

where λ_1 is the upstream mean free path which is a natural choice for a characteristic length-scale as changes through the shock occur due to few collisions and $c_1 = \sqrt{\gamma \mathcal{R} T_1}$ being the adiabatic sound speed. Further, we assume that the molecular mass diffusivity coefficient κ_m is related to the viscosity coefficient via the relation, $\kappa_m = -\kappa_{m_0} \mu / \rho$ with κ_{m_0} being a constant. Hence, the dimensionless forms of transport coefficients $\bar{\kappa}$ and $\bar{\kappa}_m$ are:

$$\bar{\kappa} = \frac{\gamma}{(\gamma - 1) \text{Pr}} \bar{\mu} \quad \text{and} \quad \bar{\kappa}_m = -\kappa_{m_0} \frac{\bar{\mu}}{\bar{\rho}}, \quad (25)$$

where Pr is the Prandtl number whose value is equal to 2/3 for the case of a monatomic gas.

It is well-known that the viscosity and temperature relation has a noticeable effect on the shock wave structure. Here we adopt the generally accepted temperature-dependent viscosity power law [6, 16]: $\mu \propto T^s$ or $\mu = \alpha T^s$, where α is a constant of proportionality taken to be γ^s and the power s for almost all real gases falling between $0.5 \leq s \leq 1$, with the limiting cases, $s = 0.5$ and $s = 1$ corresponding to theoretical gases, namely, the hard-sphere and Maxwellian gases, respectively. In our simulations we use $s = 0.75$ for a monatomic Argon gas.

The final reduced re-casted Navier-Stokes system in terms of the dimensionless quantities defined via (24) is:

$$\begin{aligned} \left(1 + \frac{\bar{\kappa}_m}{\lambda_0 \text{Ma}_1} \frac{d\bar{\rho}}{d\bar{x}}\right) \bar{u}_v + \frac{1}{\bar{m}_0} \bar{\rho} \bar{T} + \frac{1}{\lambda_0 \text{Ma}_1} \bar{\Pi}_v^{(RNS)} - \bar{p}_0 &= 0, \\ \left(1 + \frac{\bar{\kappa}_m}{\lambda_0 \text{Ma}_1} \frac{d\bar{\rho}}{d\bar{x}}\right) \left(\frac{\gamma}{(\gamma - 1)} \bar{T} + \frac{1}{2} \bar{u}_v^2\right) - \frac{\gamma^2}{\lambda_0^3 \text{Ma}_1} \frac{\bar{\kappa}_m^3}{2 \bar{\rho}^2} \left(\frac{d\bar{\rho}}{d\bar{x}}\right)^3 \\ + \frac{1}{\lambda_0 \text{Ma}_1} \left(\bar{\Pi}_v - \frac{3}{2} \bar{\kappa}_m \bar{u}_v \frac{d\bar{\rho}}{d\bar{x}}\right) \left(\bar{u}_v - \frac{\gamma}{\lambda_0} \frac{\bar{\kappa}_m}{\bar{\rho}} \frac{d\bar{\rho}}{d\bar{x}}\right) \\ + \frac{1}{\lambda_0 \text{Ma}_1} \bar{q}_v^{(RNS)} - \frac{1}{(\gamma - 1)} \bar{h}_0 &= 0, \end{aligned} \quad (26)$$

$$\begin{aligned} \left(1 + \frac{\bar{\kappa}_m}{\lambda_0 \text{Ma}_1} \frac{d\bar{\rho}}{d\bar{x}}\right) \left(\frac{\gamma}{(\gamma - 1)} \bar{T} + \frac{1}{2} \bar{u}_v^2\right) - \frac{\gamma^2}{\lambda_0^3 \text{Ma}_1} \frac{\bar{\kappa}_m^3}{2 \bar{\rho}^2} \left(\frac{d\bar{\rho}}{d\bar{x}}\right)^3 \\ + \frac{1}{\lambda_0 \text{Ma}_1} \left(\bar{\Pi}_v - \frac{3}{2} \bar{\kappa}_m \bar{u}_v \frac{d\bar{\rho}}{d\bar{x}}\right) \left(\bar{u}_v - \frac{\gamma}{\lambda_0} \frac{\bar{\kappa}_m}{\bar{\rho}} \frac{d\bar{\rho}}{d\bar{x}}\right) \\ + \frac{1}{\lambda_0 \text{Ma}_1} \bar{q}_v^{(RNS)} - \frac{1}{(\gamma - 1)} \bar{h}_0 &= 0, \end{aligned} \quad (27)$$

where Ma_1 is the upstream Mach number defined as, $\text{Ma}_1 = u_{v1}/c_1$. Quantities \bar{m}_0 , \bar{p}_0 and \bar{h}_0 are integration constants whose expressions are obtained using the well-known Rankine-Hugoniot conditions: $\bar{m}_0 = \gamma \text{Ma}_1$, $\bar{p}_0 = (1/(\gamma \text{Ma}_1)) (1 + \gamma \text{Ma}_1^2)$, $\bar{h}_0 = 1 + ((\gamma - 1)/2) \text{Ma}_1^2$. Expressions for the dimensionless new shear stress and the new heat flux are given by,

$$\bar{\Pi}_v^{(RNS)} = \bar{\Pi}_v - 2 \bar{\kappa}_m \bar{u}_v \frac{d\bar{\rho}}{d\bar{x}} + \left(\frac{\gamma}{\lambda_0}\right) \frac{\bar{\kappa}_m^2}{\bar{\rho}} \left(\frac{d\bar{\rho}}{d\bar{x}}\right)^2, \quad (28)$$

$$\bar{q}_v^{(RNS)} = -\bar{\kappa} \frac{d\bar{T}}{d\bar{x}} - \frac{\gamma}{(\gamma - 1)} \bar{\kappa}_m \bar{T} \frac{d\bar{\rho}}{d\bar{x}}, \quad (29)$$

$$\text{with } \bar{\Pi}_v = -\frac{4}{3} \bar{\mu} \frac{d\bar{u}_v}{d\bar{x}} + \frac{4}{3} \left(\frac{\gamma}{\lambda_0}\right) \frac{\bar{\mu} \bar{\kappa}_m}{\bar{\rho}} \frac{d^2 \bar{\rho}}{d\bar{x}^2} - \frac{4}{3} \left(\frac{\gamma}{\lambda_0}\right) \frac{\bar{\mu} \bar{\kappa}_m}{\bar{\rho}^2} \left(\frac{d\bar{\rho}}{d\bar{x}}\right)^2. \quad (30)$$

We solved the final system (26)–(27) using a numerical scheme, namely, finite difference global solution (FDGS) developed by Reese *et al.* [4] with well-posed boundary conditions. The specific details of FDGS scheme can be found in [4].

IV. RESULTS AND DISCUSSION

We perform numerical simulations of stationary shock waves located at $x = 0$ using FDGS scheme by considering a computational spatial domain of length $40\lambda_1$ covering $(-20\lambda_1, 20\lambda_1)$ with 1601 spatial grid points. This is wide enough to contain the entire shock profile for $1.55 \leq \text{Ma} \leq 9$ without altering its structure. We assume the constant κ_{m_0} in the molecular mass diffusivity κ_m to be unity in all our present simulations. To compare the shock structure profiles among the theoretical and experimental data, the position x has been scaled such that $x = 0$ corresponds to a value of the normalized gas density, $\rho_N = (\rho - \rho_1)/(\rho_2 - \rho_1)$, equals 0.5.

A. Mass velocity vs volume velocity

While the re-casted Navier-Stokes and the original equations may convert into one another, velocity profile solution from the original represents the mass velocity (u), and the transformed equations gives the volume velocity (u_v). The two differ by the diffusive flux as defined in (5). These are depicted in figure 1. Both velocity profiles have been

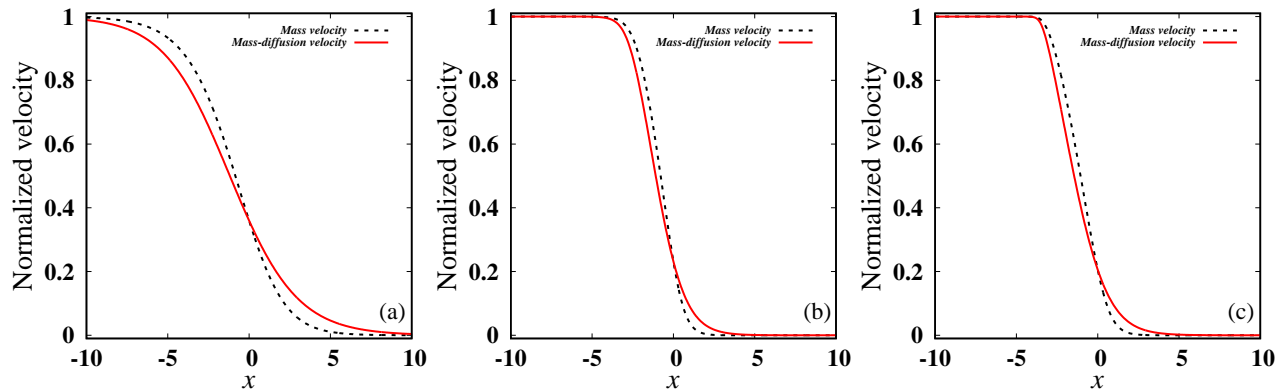


FIG. 1: Variation of normalized volume velocity (u_{v_N}) and mass velocity (u_N) profiles in Ar shock layer: for (a) $Ma_1 = 1.55$, (b) $Ma_1 = 3.8$, and (c) $Ma_1 = 9$.

normalized such that $u_N = (u - u_2)/(u_1 - u_2)$ and $u_{v_N} = (u_v - u_{v_2})/(u_{v_1} - u_{v_2})$. The volume velocity predicted by the re-casted Navier-Stokes is more flatter than the mass velocity profile, predicted by the classical NS, which is evident from figure 1. Next we show that not only the velocity profiles differ in the transformation process but the entire hydrodynamic field variables compared differently with experiments.

B. Density profiles

Full experimental data exist for monatomic gas density variations within shock layers [9]. These data are therefore our first choices for comparison. They are shock waves in Argon gas for upstream Mach numbers ranging between 1.55 and 9.

Figure 2 shows the predicted normalized density profiles through an Argon shock wave using the re-casted and the original equations with $s = 0.75$ compared with the experimentally measured density data. Panels (a), (b), (c), (d), (e) and (f) of figure 2 correspond to upstream Mach numbers of $Ma_1 = 1.55, 2.05, 3.38, 3.8, 6.5$, and 9 , respectively. In each panel, the dotted black lines represent solutions of the Navier-Stokes equations and the solid red lines represent solutions by the re-casted Navier-Stokes equations. The filled blue circles represent the experimental data. For the upstream Mach number of 1.55, one observes from panel (a) of figure 2 that classical Navier-Stokes predict the upstream shock layer as the experiments but completely fail to predict the downstream shock layer. The re-casted Navier-Stokes equations produce good agreement with the experimental data with a small disparity at the upstream shock layer and is more flatter than the experimental data. The re-casted Navier-Stokes predictions for the normalized density profiles show excellent agreement with the experimental data for the upstream Mach number of $Ma_1 = 2.05, 3.38$ and 3.8 , which is evident from panels (b)-(d) of figure 2. In fact, a good agreement between predictions of the re-casted Navier-Stokes equations and the experimental data of Alsmeyer [9] is found for upstream Mach number from 2 to 5. At the high upstream Mach numbers $Ma_1 = 6.5$, figure 2(e) and $Ma_1 = 9$, figure 2(f), the predictions of re-casted Navier-Stokes equations for the variation of the density within the shock layer are still better compared to the original equations. At the upstream Mach number of 6.5 and 9, the re-casted Navier-Stokes predictions are less flatter than the experimental predictions at the upstream part of the shock. Overall, the re-casted Navier-Stokes solutions are better than the original at all upstream Mach numbers.

C. Reciprocal shock thickness

Generally, studies of shock structures consist of validating by comparing a few shock structure parameters with experimental data, where available, and other numerical simulations. One of the principal parameter of shock structure is the non-dimensional inverse shock thickness $\delta = \lambda_1/L$, where the shock thickness or shock width is defined as [6, 9]:

$$L = \frac{\rho_2 - \rho_1}{|\max(\frac{d\rho}{dx})|}, \quad (31)$$

and is based on the density profile and depends mainly on the central part of the shock wave. The reciprocal shock thickness (δ) is one of the widely used shock parameter to compare computational results with experiments

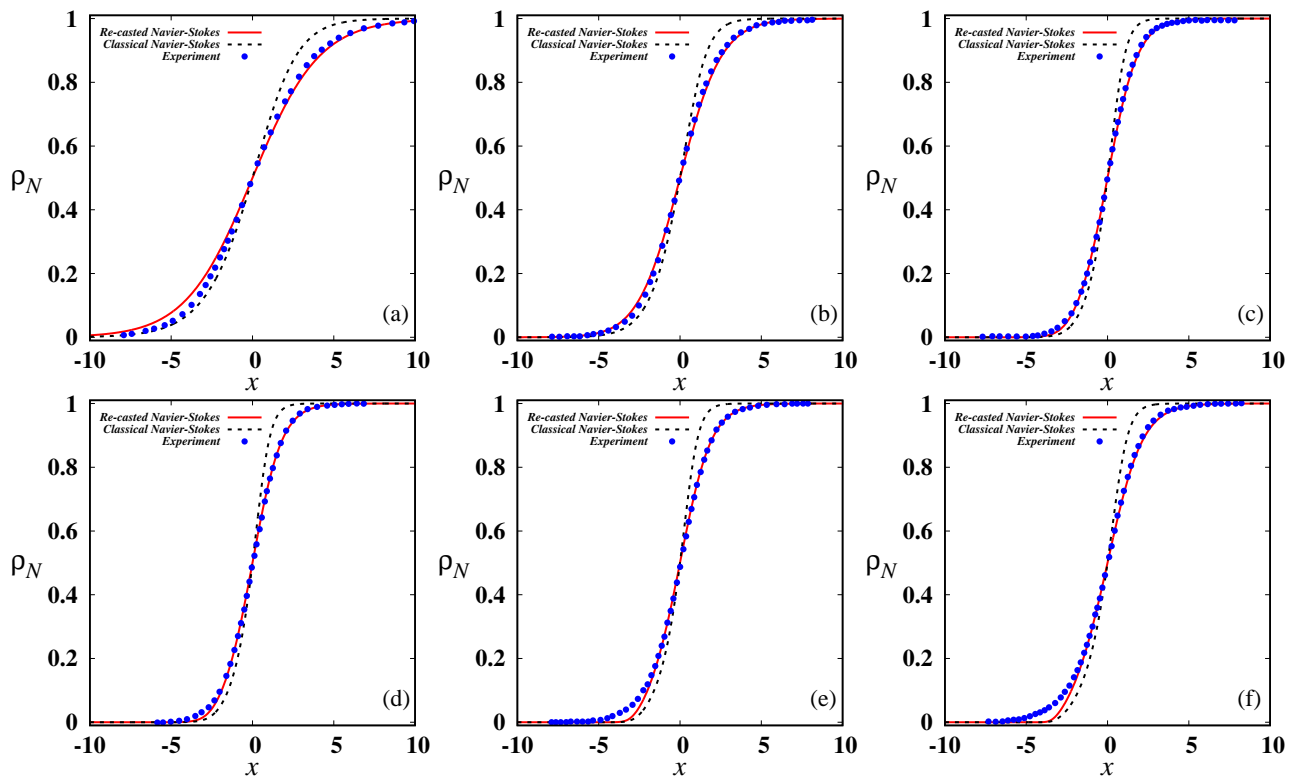


FIG. 2: Variation of normalized density (ρ_N) profiles in Ar shock layer: for (a) $Ma_1 = 1.55$, (b) $Ma_1 = 2.05$, (c) $Ma_1 = 3.38$, (d) $Ma_1 = 3.8$, (e) $Ma_1 = 6.5$ and (f) $Ma_1 = 9$. In each panel, the dotted black line represents the solution of classical Navier-Stokes equations, the solid red line represents the solutions of re-casted Navier-Stokes equations and the filled blue circles represent experimental data of Alsmeyer [9].

as it possesses an important feature that is, it represents actually the Knudsen number of the shock structure flow problem. In other words, the shock thickness acts as the characteristic dimension of the flow configuration [6].

The most comprehensive collection of experimental data for the reciprocal shock thickness (δ) is reported in [9]. Figure 3(a) shows predictions of re-casted Navier-Stokes equations for the reciprocal shock thickness (the inverse density thickness) in Argon for an upstream Mach number up to $Ma_1 = 11$, with experimental data assembled from Alsmeyer [9]. Predictions from the classical Navier-Stokes are also presented for the sake of completeness. From figure 3(a), one can observe that the classical Navier-Stokes equations with $s = 0.75$ (see black dotted line) and with $s = 0.72$ (see red dotted line) predict the reciprocal shock thickness to be 1.4 to 2 times the measured over the entire Mach number range presented. However, the solution from the re-casted Navier-Stokes equations with the choice of $\kappa_{m_0} = 1$ and $s = 0.75$ is found to follow closely the experimental results of Alsmeyer [9]. It is noteworthy to mention that for $\kappa_{m_0} = 0$, the results using the re-casted NS coincides with that of the classical NS results.

D. Asymmetry quotient of density profile

From figure 2, at the upstream part of the profile one can observe that there are still some discrepancies between predictions and experimental shock density profiles at some Mach numbers. However, the results by the reciprocal shock thickness δ conclude that the re-casted Navier-Stokes equations showed excellent prediction of the experimental data. This suggests that the inverse density thickness δ does not express full information about the overall shape of the shock wave profile, as it just depends on the maximum density gradient alone.

A second important measure of a shock structure for which experimental results are available is the asymmetry of the density profile, Q . This gives more information about the shape of the shock profile as it measures skewness of the density profile relative to its midpoint [6]. The shock asymmetry, Q , is defined based on the normalized density

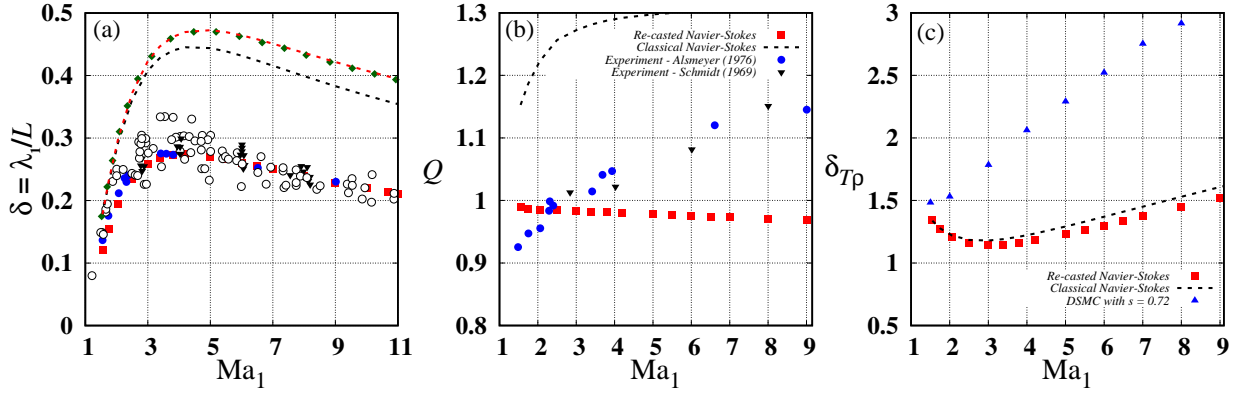


FIG. 3: Variation of the different shock structure parameters for monatomic gas, Ar: (a) reciprocal shock width (δ), (b) density asymmetry quotient (Q), and (c) temperature-density spatial lag ($\delta_{T\rho}$). Theoretical results: \blacksquare – re-casted Navier-Stokes solution with $\kappa_{m_0} = 1$ and $s = 0.75$, black and red dotted lines show present solutions of the NS with $s = 0.75$ and $s = 0.72$, respectively, using FDGS technique, \blacklozenge – NS solution of Paolucci and Paolucci [10] with $s = 0.72$; experimental results: \circ – Alsmeyer [9], \blacktriangledown – Schmidt (1969) and \circ – other experimental data assembled from Alsmeyer [9]; \blacktriangle – DSMC results with $s = 0.72$ taken from Lumpkin and Chapman [16].

profile, ρ_N , with its centre, $\rho_N = 0.5$, located at $x = 0$, as

$$Q = \frac{\int_{-\infty}^0 \rho_N(x) dx}{\int_0^{\infty} [1 - \rho_N(x)] dx}. \quad (32)$$

From definition (32) it is clear that, a symmetric shock wave will have a density asymmetry quotient of unity, while for realistic shock waves its value is around unity as shocks are not completely symmetric about their midpoint. Figure 3(b) shows predictions of the re-casted Navier-Stokes and the Navier-Stokes equations for the asymmetry quotient compared with experimental data of Alsmeyer [9] and Schmidt [17]. The classical Navier-Stokes equations predict an asymmetry quotient of more than unity at all Mach numbers and these results are no way in agreement with the experiments. This is evident from panel (b) of figure 3. The re-casted Navier-Stokes predict an asymmetry quotient of around unity at all upstream Mach numbers ($0.95 \lesssim Q \lesssim 1$). From this, one can conclude that density profiles predicted by the re-casted Navier-Stokes are almost symmetric about their midpoint.

E. Spatial lag of temperature-density profiles

Another shock structure parameter is defined based on the spatial difference between the temperature and density shock profiles. Due to the different finite relaxation times between momentum transport and energy transport, variation in density and temperature within a shock does not occur at the same time. Spatial density changes occur after temperature changes. Hence, the spatial difference, $\delta_{T\rho}$, between the normalized density and temperature profiles is defined by,

$$\delta_{T\rho} = |x(0.5 T_N) - x(0.5 \rho_N)|, \quad (33)$$

where, $T_N = (T - T_1)/(T_2 - T_1)$ is the normalized temperature. From definition (33) it is clear that the temperature-density separation measures the distance between the midpoints of the respective normalized profiles. Due to lack of experimental data for this shock structure parameter, we utilize the available DSMC data [6, 16] to compare with the predictions by the theoretical models.

Figure 3(c) compares results between the re-casted and the classical Navier-stokes equations along with DSMC data of Lumpkin and Chapman [16] for the shock macroscopic parameter temperature-density separation, $\delta_{T\rho}$. The DSMC data with a viscosity-temperature exponent $s = 0.72$ shows that $\delta_{T\rho}$ value increases with increasing Mach number, in particular increases from ≈ 1.5 to ≈ 2.9 when Mach number increases from 1.5 to 8, as it can be seen from panel (c) of figure 3. Results by re-casted Navier-Stokes equations quantitatively follow that of the classical. Both classical and re-casted Navier-Stokes equations under predicts $\delta_{T\rho}$ at all upstream Mach numbers. One can observe that the hydrodynamic equations (classical and re-casted) show a decreasing $\delta_{T\rho}$ for $1.5 \leq Ma_1 \leq 3$ and then the value of $\delta_{T\rho}$ increases for $Ma_1 > 3$. Generally, as explicit experimental data are not available for temperature profiles it is inconvenient to conclude which model predicts the accurate temperature-density separation from figure 3(c).

V. CONCLUSIONS

The stationary shock structure problem in a monatomic gas (Argon) is analyzed by numerically solving the classical and re-casted Navier-Stokes equations. We observed that solutions as given by the re-casted Navier-Stokes equations differ from solutions by the original. The difference is attributable to the fact that hydrodynamic field variables from the re-casted equations no longer operate as in the original equations (also as boundary conditions are set based on redefined hydrodynamic variables rather than those in the original equations). The re-casted Navier-Stokes equations with a constant in the mass diffusion coefficient, $\kappa_{m_0} = 1$, and a viscosity-temperature exponent, $s = 0.75$, show better agreements with Alsmeyer [9] experimentally measured density profiles in Argon gas. In the case of the reciprocal shock thickness re-casted Navier-Stokes delivered an excellent match with Alsmeyer [9] experimental data and exactly coincides with the experimental results at large upstream Mach numbers. However, it does not reproduce the more detailed density asymmetry quotient and temperature-density separation. Nevertheless, we conclude that the re-casted Navier-Stokes equations better reproduce the shock profiles experimental data. We therefore suggest further investigation and examination of the re-casted model on other non-equilibrium gas flow configurations.

ACKNOWLEDGMENTS

This research is supported by the UK's Engineering and Physical Sciences Research Council (EPSRC) under grant no. EP/R008027/1 and The Leverhulme Trust, UK, under grant Ref. RPG-2018-174.

-
- [1] R. Courant and K. O. Friedrichs, *Supersonic Flow and Shock Waves* (New York: Interscience, 1948).
 - [2] H. Grad, The profile of a steady plane shock wave, *Commun. Pure Appl. Math.* **5**, 257 (1952).
 - [3] G. A. Bird, *Molecular Gas Dynamics and the Direct Simulation of Gas Flows* (Oxford Univ Press, 1994).
 - [4] J. M. Reese, L. C. Woods, F. J. P. Thivet, and S. M. Candel, A second-order description of shock structure, *J. Comput. Phys.* **117**, 240 (1995).
 - [5] M. H. L. Reddy and M. Alam, Plane shock waves and Haff's law in a granular gas, *J. Fluid Mech.* **779**, R2 (2015).
 - [6] C. J. Greenshields and J. M. Reese, The structure of shock waves as a test of Brenner's modifications to the Navier-Stokes equations, *J. Fluid Mech.* **580**, 407 (2007).
 - [7] M. H. L. Reddy, *Plane shock waves in granular gases and regularized moment equations*, Ph.D. thesis, Jawaharlal Nehru Centre for Advanced Scientific Research, India (2016).
 - [8] R. J. LeVeque, *Finite Volume Methods for Hyperbolic Problems* (Cambridge University Press, 2002).
 - [9] H. Alsmeyer, Density profiles in argon and nitrogen shock waves measured by the absorption of an electron beam, *J. Fluid Mech.* **74**, 497 (1976).
 - [10] S. Paolucci and C. Paolucci, A second-order continuum theory of fluids, *J. Fluid Mech.* **846**, 686 (2018).
 - [11] H. Brenner, Beyond Navier-Stokes, *Int. J. Eng. Sci.* **54**, 67 (2012).
 - [12] C. Calgaro, E. Creusé, and T. Goudon, Modeling and simulation of mixture flows: Application to powder-snow avalanches, *Computers & Fluids* **107**, 100 (2015).
 - [13] S. K. Dadzie, J. M. Reese, and C. R. McInnes, A continuum model of gas flows with localized density variations, *Physica A* **387**, 6079 (2008).
 - [14] T. Koide and T. Kodama, Generalization of uncertainty relation for quantum and stochastic systems, *Phys. Lett* **382**, 1472 (2018).
 - [15] H. W. Liepmann and A. Roshko, *Elements of Gas Dynamics* (John Wiley & Sons, Inc., New York, 1957).
 - [16] F. E. Lumpkin and D. R. Chapman, Accuracy of the burnett equations for hypersonic real gas flows, *AIAA Paper* , 91 (1991).
 - [17] B. Schmidt, Electron beam density measurements in shock waves in argon, *J. Fluid Mech.* **39**, 361 (1969).